

kalis: A Modern Implementation of the Li & Stephens Model for Local Ancestry Inference in R

Louis J.M. Aslett^{1*} and Ryan R. Christ²

^{1*}Department of Mathematical Sciences, Durham University, Stockton Road, Durham, DH1 3LE, County Durham, UK.

²Department of Genetics, Yale School of Medicine, 333 Cedar Street, New Haven, 06520, CT, USA.

*Corresponding author(s). E-mail(s): louis.aslett@durham.ac.uk;
Contributing authors: ryan.christ@yale.edu;

Abstract

Background Approximating the recent phylogeny of N phased haplotypes at a set of variants along the genome is a core problem in modern population genomics and central to performing genome-wide screens for association, selection, introgression, and other signals. The Li & Stephens (LS) model provides a simple yet powerful hidden Markov model for inferring the recent ancestry at a given variant, represented as an $N \times N$ distance matrix based on posterior decodings.

Results We provide a high-performance engine to make these posterior decodings readily accessible with minimal pre-processing via an easy to use package **kalis**, in the statistical programming language R. **kalis** enables investigators to rapidly resolve the ancestry at loci of interest and developers to build a range of variant-specific ancestral inference pipelines on top. **kalis** exploits both multi-core parallelism and modern CPU vector instruction sets to enable scaling to hundreds of thousands of genomes.

Conclusions The resulting distance matrices accessible via **kalis** enable local ancestry, selection, and association studies in modern large scale genomic datasets.

Keywords: Li & Stephens Model, R package, probabilistic haplotype model, Hidden Markov Model, genomics, high performance computation

047 Background

048
049 The hidden Markov model (HMM) of haplotype diversity proposed by Li & Stephens
050
051 [1] (hereinafter, the LS model) has become the basis for several probabilistic phasing,
052
053 ancestry inference, and demographic inference methods in modern genomics [2, 3].

054 ~~The LS model provides the basis for the genome-wide~~

055
056 Accelerated implementations of the LS model, typically targeting the Viterbi
057 path, are integral to many commonly used genomics software packages, including
058 BEAGLE [4], IMPUTE [5], and tsinfer [6]. A pioneering ancestry inference software
059 ChromoPainter, which summarizes the package, ChromoPainter, popularized the idea
060 of using the LS model to summarize the ancestry of N haplotypes with an $N \times N$
061 similarity matrix [7]. This matrix is obtained by running N independent HMMs in
062
063 which each haplotype is modelled as a mosaic of all of the other haplotypes in the
064
065 sample. This ‘*all-vs-all*’ copying approach is motivated by the product of approximate
066
067 conditionals (PAC) likelihood originally proposed by [1] and allows ChromoPainter to
068
069 render a chromosome-wide estimate of the recent ancestry of the N haplotypes with
070
071 high resolution.

072
073
074 ~~Beyond chromosome-wide summaries, the LS model can also be used for~~
075 ~~variant-specific ancestry inference. The contemporary importance of this is highlighted~~
076 ~~by the recent advances achieved in the RELATE software suite [2], which uses the~~
077 ~~LS model internally to~~ The Relate [2] software suite extended this idea to performing
078
079 local (locus-specific) ancestry inference along the genome. Internally, Relate uses high
080 performance C++ implementations of the forward and backward algorithm to perform
081 posterior decoding under a modified version of the LS model that incorporates derived
082 allele information at many loci spaced along the genome. We will refer to this modified
083 LS model as the derived allele haplotype copying model. These posterior decodings are
084
085
086
087
088
089
090
091
092

transformed to $N \times N$ local genetic distance matrices and used to initialise variant-specific ancestral trees for downstream population genetic analyses ranging from demography to selection inference.

The current Relate software suite does not provide an interface for outputting the posterior decodings at a locus of interest and does not support the original LS model, only the derived allele haplotype copying model, which requires derived allele information.

Additionally, a LS-like model is implemented in [8] to run forward and backward recursions to variants of interest. However, the transition kernel used is different to the original LS model: upon a recombination event the transition kernel in [8] does not permit a haplotype to continue copying from the same donor haplotype.

The focus of **kalis** ~~focuses on providing~~ is to provide a high-performance engine to ~~compute exclusively the LS model, enabling users to rapidly develop~~ directly obtain the posterior decoding at a set of loci of interest for a dataset with hundreds of thousands of phased haplotypes. **kalis** supports the original LS model and the derived allele haplotype copying model. It provides a simple interface to enable rapid development of a range of future variant-specific ancestral inference pipelines on top, in the easy to use statistical programming language R [9].

At the same time, it has been recognised for over a decade [10] that the serial execution speed of CPUs will increase modestly, with additional performance primarily coming from concurrency via multi-core architectures or the growing width of specialised single instruction, multiple data (SIMD) instruction sets. Whilst multi-core architectures are now somewhat routinely exploited via forked processes or threading, SIMD instructions remain an often overlooked source of performance gains, possibly because they are harder to program. There are a cornucopia of SIMD instruction sets: on the Intel platform the genesis was in the 64-bit wide MMX instruction set [11] which allows simultaneous operation on two 32-bit, four 16-bit or eight 8-bit integers.

139 The most recent incarnation on Intel CPUs is a suite of AVX-512 instruction sets [12],
140 now capable of operating on 512-bits of various data types simultaneously (eg eight
141 64-bit floating point, or sixteen 32-bit integer values). Other CPU designs have similar
142 SIMD technologies, such as NEON on ARM CPU [13] designs (including the Apple M1
143 and M2 processors, as well as Amazon Web Services Graviton range). Additionally all
144 modern CPUs are superscalar architectures supporting instruction level parallelism,
145 an advance that has been in the consumer Intel platform since the Pentium [14]. Judi-
146 cious programming can make it easier for compilers and the deep reorder buffers of
147 modern pipelined CPUs to exploit this more hidden form of parallelism.

154 In this work we provide a reformulation of the LS model and an optimised memory
155 representation for haplotypes, which together enable us to leverage *both* multi-core
156 and SIMD vector instruction parallelism to obtain local genetic distance matrices for
157 problem sizes that previously appeared out of reach. This high performance imple-
158 mentation is programmed in C [15], with an easy to use interface provided in R [9]. We
159 provide low-level targets of AVX2, AVX-512 and NEON instruction sets (covering the
160 vast majority of CPUs in use today), and the whole package has an extensive suite of
161 162,835 unit tests.

167 In the Implementation section below, we start with a description of the LS model
168 and our reformulation which makes it amenable to these high-performance CPU
169 technologies. We also describe the technical details of the underlying low-level imple-
170 mentation for the interested reader. We then demonstrate the performance that can
171 be achieved with **kalis**, including examples with 100,000 haplotypes capable of running
172 on a single machine. To the best of our knowledge, this is the first example of running
173 the LS model at the scale of hundreds-of-thousands of haplotypes. We also present a
174 real data example using **kalis** to examine the ancestry at the *LCT* gene. In the follow-
175 ing Discussion section, we describe the user friendly R interface which enables easy
176

182
183
184

use of the high performance implementation without any knowledge of the underlying
CPU technologies.

Implementation

The LS model

To formalize our objective, let h be an $L \times N$ matrix of 0s and 1s encoding N phased
haplotypes at L sites. Let $h_i^\ell \in \{0, 1\}$ denote the (ℓ, i) th element of h . For brevity,
let h_i denote the i th haplotype (the i th column of h) and h_{-i} denote all of the
haplotypes excluding the i th haplotype. The LS model proposes an HMM for $h_i|h_{-i}$
in which the hidden state at variant ℓ , $X_i^\ell \in \{1, \dots, N\} \setminus i$, is an index indicating the
haplotype in h_{-i} that h_i is most closely related to (or “copies from”) at variant ℓ .
We present here their proposed emission and transition kernels (see Equation A1 and
Equation A2 in [1]) with a simplified parametrisation that is similar, but not identical,
to that used by ChromoPainter.

While the original LS model assumes that each haplotype has an equal *a pri-*
ori probability of copying from any other, following ChromoPainter, we define a left
stochastic matrix of prior copying probabilities $\Pi \in \mathbb{R}^{N \times N}$ where Π_{ji} is the prior
probability that haplotype j is copied by i and, by convention, $\Pi_{ii} = 0$. In other
words, the donor haplotype (hidden state) that is sampled at the first variant and
after every “recombination event” in the copying path is drawn according to Π . Here
and whenever possible in **kalis**, all matrices are column-oriented such that the i th col-
umn pertains to an independent HMM where h_i is treated as the observation. There
is some probability of a mis-copy at variant ℓ , μ^ℓ , which under the LS model is set

231 proportional to the mutation rate at ℓ . This leads to an emission kernel of the form

$$\theta_{ji}^\ell := \mathbb{P}(h_i^\ell | X_i^\ell = j) = \begin{cases} 1 - \mu^\ell & \text{if } h_i^\ell = h_j^\ell \\ \mu^\ell & \text{if } h_i^\ell \neq h_j^\ell \end{cases}. \quad (1)$$

239 The transition kernel between hidden states is based on the recombination rate
 240 between sites. Let m^l be the genetic distance between variant l and variant $l + 1$ in
 241 Morgans (the expected number of recombination events per meiosis). Define $N_e =$
 242 $4\tilde{N}_e/N$ where \tilde{N}_e is the effective diploid population size (ie half of the haploid effective
 243 population size). Then, under the LS model the transition kernel is

$$P(X_i^\ell = k | X_i^{\ell-1} = j) = \Pi_{ki} \rho_{-}^{\ell\ell-1} + \mathbf{1}\{k = j\} (1 - \rho_{-}^{\ell\ell-1}), \quad (2)$$

252 where $\rho^\ell = 1 - \exp(-N_e m^\ell)$ and $\mathbf{1}\{\cdot\}$ is the indicator function. ~~[1]~~ Intuitively,
 253 this transition kernel asserts that upon a “recombination event,” where a recipient
 254 haplotype i may change the donor haplotype j it is copying from, the new donor
 255 haplotype is resampled from the prior copying distribution $\Pi_{i\cdot}$. [1, Appendix B]
 256 observe that in practice the estimation of recombination rates ~~is~~ can be improved when
 257 the scaled recombination rate is raised to a power, so we adopt this approach and
 258 introduce an exponent γ . By default, **kalis** sets $\gamma = 1$, but this can be changed by the
 259 user. For $\gamma > 1$ the recombination map becomes more heavily peaked, whereas $\gamma < 1$
 260 tempers the recombination map to make it more flat and smooth. Hence, in **kalis**, we
 261 set

$$\rho^\ell := 1 - \exp\left(-N_e (m^\ell)^\gamma\right), \quad (3)$$

271 calculated using `expm1()` to help avoid underflow.

273 In keeping with the nomenclature introduced by [7], we refer to h_i as the “recipient
 274 haplotype” and the remaining haplotypes, h_{-i} , as the “donor haplotypes”, in the
 275
 276

context of the HMM where h_i is treated as the emitted observation vector. This reflects the fact that each recipient haplotype h_i is modelled as an imperfectly copied mosaic of the other observed haplotypes under the LS model. Hence, the posterior marginal probability at variant ℓ , $p_{ji}^\ell := \mathbb{P}(X_i^\ell = j | h)$, is the probability that donor j is copied by recipient i at variant ℓ given the haplotypes h . Under the above definitions of the prior copying probabilities Π , the emission kernel (1), and the transition kernel (2), the full $N \times N$ matrix of copying probabilities at ℓ , p^ℓ , can be obtained by running the standard forward and backward recursions [16] for each column (ie for each independent HMM).

From these posterior probabilities, we calculate a local $N \times N$ distance matrix, d^ℓ . Firstly, notice that theoretically $p_{ij}^\ell > 0$, but it can be that $p_{ij}^\ell < \varepsilon$, where ε is the double precision machine epsilon ($\approx 2.22 \times 10^{-16}$, [15], pp.26). Effectively this means d_{ij}^ℓ is too large to reliably work with precisely, and so for the purposes of distance calculations we treat ε as the smallest observable posterior probability, yielding

$$d_{ji}^\ell = -\frac{\log(p_{ji}^\ell \vee \varepsilon) + \log(p_{ij}^\ell \vee \varepsilon)}{2} \quad \forall j \neq i \quad (4)$$

where \vee is the maximum binary operator. By convention $d_{ii} = 0$ for all i .

We proceed in the next Section to reformulate the forward and backward recursions so that we can more fully exploit modern high-performance CPU instruction sets, while preserving numerical precision.

Modification of the forward-backward algorithm

The N independent HMMs of the LS model have forward and backward probabilities, respectively:

$$\tilde{\alpha}_{ji}^\ell = \mathbb{P}(X_i^\ell = j, h_i^{1:\ell}), \quad \tilde{\beta}_{ji}^\ell = \mathbb{P}(h_i^{\ell+1:L} | X_i^\ell = j), \quad i \in \{1, \dots, N\},$$

where $h_i^{1:\ell}$ denotes haplotype i from variant 1 to ℓ inclusive.

Define,

$$F_i^\ell := \sum_{j=1}^N \tilde{\alpha}_{ji}^\ell \quad F_i^0 := 1 \quad (5)$$

$$G_i^\ell := \sum_{j=1}^N \tilde{\beta}_{ji}^{\ell+1} \theta_{ji}^{\ell+1} \underline{\pi} \underline{\Pi}_{ji} \quad G_i^L := 1 \quad (6)$$

Then the forward and backward recursions for the LS model can be written in vector notation (subscript \cdot denoting a vectorised index),

$$\tilde{\alpha}_{\cdot i}^\ell \leftarrow \theta_{\cdot i}^\ell \left((1 - \rho^{\ell-1}) \tilde{\alpha}_{\cdot i}^{\ell-1} + \rho^{\ell-1} F_i^{\ell-1} \underline{\pi} \underline{\Pi}_{\cdot i} \right) \quad \text{for } \ell \in \{2, \dots, L\}, \quad (7)$$

$$\tilde{\beta}_{\cdot i}^\ell \leftarrow (1 - \rho^\ell) \tilde{\beta}_{\cdot i}^{\ell+1} \theta_{\cdot i}^{\ell+1} + \rho^\ell G_i^\ell \quad \text{for } \ell \in \{1, \dots, L-1\}. \quad (8)$$

with recursions initialised with $\alpha_{\cdot i}^1 \leftarrow \theta_{\cdot i}^1 \underline{\pi} \underline{\Pi}_{\cdot i}$ and $\beta_{\cdot i}^L \leftarrow 1$. Note that Equation (7) corresponds to Equation A5 in [1].

To partially mitigate the risk of underflow, the forward recursion can be rearranged in terms of $\alpha_{\cdot i}^\ell := \frac{\tilde{\alpha}_{\cdot i}^\ell}{F_i^{\ell-1}}$, and the backward recursion in terms of $\beta_{\cdot i}^\ell := \frac{\tilde{\beta}_{\cdot i}^\ell}{G_i^\ell}$ (see Additional file 1 for details). Thus, in full for $\ell \in \{1, \dots, L\}$ we compute,

$$\alpha_{\cdot i}^1 \leftarrow \theta_{\cdot i}^1 \underline{\pi} \underline{\Pi}_{\cdot i} \quad \text{for } \ell = 1 \quad (9)$$

$$\alpha_{\cdot i}^\ell \leftarrow \theta_{\cdot i}^\ell \left((1 - \rho^{\ell-1}) \frac{\alpha_{\cdot i}^{\ell-1}}{\sum_j \alpha_{ji}^{\ell-1}} + \rho^{\ell-1} \underline{\pi} \underline{\Pi}_{\cdot i} \right) \quad \text{for } \ell > 1 \quad (10)$$

and

$$\beta_{\cdot i}^L \leftarrow 1 \quad \text{for } \ell = L \quad (11)$$

$$\beta_i^\ell \leftarrow (1 - \rho^\ell) \frac{\beta_i^{\ell+1} \theta_i^{\ell+1}}{\sum_j \beta_{ji}^{\ell+1} \theta_{ji}^{\ell+1} \pi_{ji}} \frac{\beta_i^{\ell+1} \theta_i^{\ell+1}}{\sum_j \beta_{ji}^{\ell+1} \theta_{ji}^{\ell+1} \Pi_{ji}} + \rho^\ell \quad \text{for } \ell < L \quad (12)$$

Given α_i^ℓ and β_i^ℓ , the vector of posterior probabilities for recipient i , p_i^ℓ , can be calculated directly by normalising,

$$p_i^\ell = \frac{\alpha_i^\ell \odot \beta_i^\ell}{\sum_j \alpha_{ji}^\ell \odot \beta_{ji}^\ell} \quad (13)$$

where \odot denotes the Hadamard product. In the event that $\sum_j \alpha_{ji}^\ell \odot \beta_{ji}^\ell = 0$, the distance between the recipient haplotype i and all of the donor haplotypes is beyond numerical precision, so as per the earlier discussion we define $p_{ji}^\ell = \varepsilon \forall j \neq i$.

Finally, the local distances follow by taking the negative log and symmetrising. Note that if the distances are standardised for one of these columns, to account for the fact that the standard deviation will be 0, we set all of the standardised distances to 0. Please see Additional file 1 for a discussion on parameter values and exactly how **kalis** performs certain computations to maintain the numerical stability of the algorithm.

Core Implementation Details

The R interface described hereinbefore is a thin wrapper layer around a high-performance implementation of the core algorithm which is written in standards compliant C18 [15]. Most data structures are represented with native R types enabling user inspection and manipulation, except for the haplotype sequences themselves.

Computationally, the innermost forward and backward recursions are implemented using compiler intrinsics to exploit a variety of modern CPU instruction sets, including Streaming SIMD Extensions (SSE2 and SSE4.1), Advanced Vector Extensions (AVX, AVX2, AVX-512 and FMA) and Bit Manipulation Instructions (BMI2) on Intel platforms; as well as NEON on ARM platforms. AVX2 is supported in Intel CPUs of the

415 Haswell generation (released Q2 of 2013) or later, AVX-512 tends to be available only
416 in recent Intel server and workstation grade CPUs, and NEON is available for ARM
417 Cortex-A and Cortex-R series CPUs, as well as Apple M1/M2 and Amazon Web Ser-
418 vices Graviton processors. Although this covers most CPUs likely to be in use today,
419 we none-the-less provide reference implementations in pure standards compliant C
420 which will operate on any CPU architecture with a C18 compliant compiler. During
421 package compilation, the correct code-paths are compiled based on detection of the
422 presence or absence of the required instruction sets, or at the direction of the user
423 via compiler flags. See Additional file 1 for more details, and for guidance on how to
424 directly check your CPU for SIMD support.

431 It may be worth noting at this juncture that it was an explicit design choice to tar-
432 get CPUs and not GPU or tensor cards initially. This is because most University high
433 performance computing clusters have plentiful CPU resources, often with untapped
434 power in advanced SIMD instructions sets. We believe that the problem size that can
435 be realistically tackled in many genetics studies can be massively increased *without*
436 needing to resort to add-on cards, though to scale beyond even this we may explore
437 heterogeneous computing architectures in future **kalis** research.

443 In this section, we now describe the inner workings and design principles of the
444 package, first covering in detail the data structures (both user facing and internal),
445 followed by the computational implementation.

449 Data structures

451 There are three user accessible data structures utilised in the package and a low
452 level binary haplotype representation which is not directly user accessible. The two
453 principle data structures of interest to users are forward and backward table objects,
454 represented as native R lists with respective S3 class names **kalisForwardTable** and
455 **kalisBackwardTable** (detailed in Table 2 and discussed later), which are created with
456
457
458
459
460

package functions `MakeForwardTable()` and `MakeBackwardTable()` respectively. The third user accessible data structure holds the LS model parameters, represented as a native R environment with S3 class name `kalisParameters`, which can be created with the package function `Parameters()`.

Haplotype data

The haplotypes are stored in an optimised binary representation which is only natively accessible from within C. Note that here “optimised” is not a reference to space-optimisation: it would be possible to represent the haplotypes in an even more compressed manner, but we aim for streaming compute speed optimisation instead.

The haplotypes are loaded from disk and transformed to an in memory cache in this representation via `CacheHaplotypes()`, but this function does not return any handle to the loaded data. Thus the package provides the accessor function `QueryCache()`, which copies genome segments from the binary representation into native R integer vectors for user inspection.

When `CacheHaplotypes()` loads haplotypes into the cache, they are interleaved into a flat memory space which is organised as variant-major. That is, variant 1 of each haplotype is loaded, converted to a binary 0/1 and then 32 consecutive haplotypes are packed into an unsigned integer. Moreover, the initial flat memory allocation is aligned on a 32-byte boundary to satisfy memory alignment requirements for some CPU vector instructions¹, and after all haplotypes at a given variant are packed into consecutive unsigned integers the pointer is wound forward to the next 32-byte boundary to ensure the next variant starts on an SSE/AVX vector compatible memory boundary. This is depicted in Figure 1.

Firstly, note that this orientation is natural, since the forward and backward recursions operate variant by variant, meaning variant-major storage ensures sequential

¹Certain modern CPUs do not require specific alignment to be able to load memory to SSE/AVX registers, but for maximum compatibility we honor the alignment anyway.

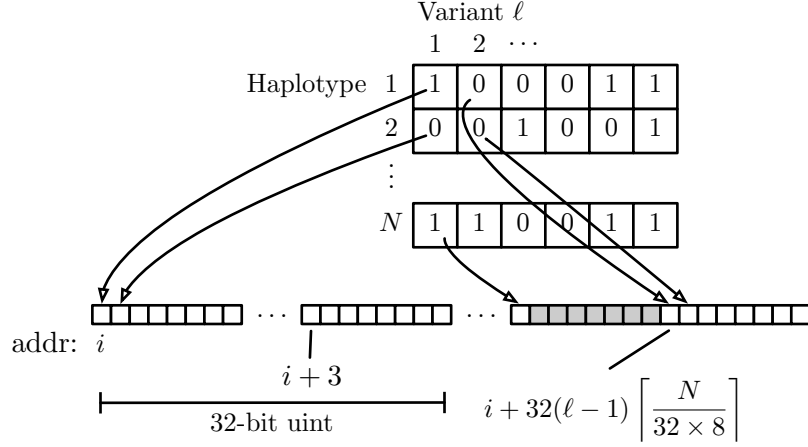


Fig. 1 Efficient binary representation of interleaved haplotypes in memory, with 32-byte boundary alignment for each variant start for SSE/AVX instructions (here $i \bmod 32 = 0$). The grey boxes indicate essentially ‘wasted’ bits which are ignored to ensure alignment for the start of the next variant.

memory locations are fetched during a recursion. Indeed, with the cache line size of 64-bytes (starting Intel Pentium IV), we essentially trigger the loading of $64 \times 8 = 512$ neighbouring variants upon accessing the first variant in a recursion. This effect is even more pronounced on Apple M1/M2 whose cache line size is 128-bytes, resulting in 1024 variants being pre-fetched upon access to the first variant in a recursion.

Secondly, a possible drawback is that we must extract the individual bit into a double floating point representation in order to compute with it in the recursion. However, efficient CPU instructions can help here too: take for example the following strategy **kalis** uses on an AVX2 capable CPU. Using the **PDEP** instruction in BMI2, we can efficiently deposit a bit into every ninth bit of an **int** (so there are now 4 8-bit integers taking on the value of the haplotype at this variant packed in an **int**). Then, using SSE2, SSE4.1 and AVX instructions one can inflate through representations from 4 8-bit integers packed in an **int** up to 4 64-bit doubles packed in a 256-bit AVX register. As such, we are then ready to operate with this variant in parallel using AVX instructions.

During development, testing indicated the memory bandwidth and cache efficiency savings of the packed binary representation provided speed-ups thanks to these instructions efficiently enabling unpacking and spreading a haplotype variant bit for parallel use. Furthermore, such a compact representation means that more of L1/L2 cache and memory bus bandwidth is left available for forward and backward tables, which are the largest objects we work with in this problem.

Parameters

The parameter set used by `kalis` can be created by calling the `Parameters()` function, which returns a `kalisParameters` object with structure shown in Table 1. This structure corresponds to the parameters required to specify the LS model (Equations (1) and (2)). To calculate ρ from a recombination map, N_e and γ , we also provide a helper function, `CalcRho()`, which implements Equation (3).

The `kalisParameters` object uses an environment rather than list for parameters for two reasons: (i) the parameter environment and its bindings are locked which prevents changes in parameter values between forward or backward table propagation steps, since parameters must be fixed for all steps of a given forward or backward computation; and (ii) an environment explicitly ensures the (often large) parameter vectors are not copied when associated with potentially many different tables, but will always be purely referenced.

The environment contains only two members: another environment with the actual parameter values (which is locked with `lockEnvironment()`); and a SHA-256 hash of those parameter values (details in Table 1). The purpose of the hash is to be able to efficiently determine whether the correct parameter set for a given forward or backward table has been passed when computing forward or backward recursions from an already initialised table (since it would be incorrect to propagate forward or backward using different parameter sets in different parts of the genome).

<code>kalisParameters</code> object	Data type
<code>pars</code>	Locked R environment, containing:
	<code>rho</code> vector length L
	<code>mu</code> vector length L , or scalar
	<code>Pi</code> $N \times N$ matrix, or scalar
<code>sha256</code>	character

Table 1 The content of the data structure representing parameter objects.

<code>kalisForwardTable</code> object	<code>kalisBackwardTable</code> object	Data type
<code>alpha</code> = α^ℓ	<code>beta</code> = β^ℓ	$N \times N$ matrix
<code>alpha.f</code> = F^ℓ	<code>beta.g</code> = G^ℓ	vector length N
<code>l</code> = ℓ	<code>l</code> = ℓ	integer scalar
<code>from_recipient</code>	<code>from_recipient</code>	integer scalar
<code>to_recipient</code>	<code>to_recipient</code>	integer scalar
<code>pars.sha256</code>	<code>pars.sha256</code>	character
	<code>beta.theta</code>	logical scalar

Table 2 The content of the core data structures representing forward and backward table objects, together with their correspondence to mathematical quantities.

Forward/backward tables

Recall that the recipients (columns) in the forward/backward tables correspond to independent HMMs. Therefore, **kalis** enables storing only a ‘slice’ of recipients in a forward/backward table, making parallelisation across non-shared memory clusters much simpler: given all haplotype data, these recipient slices can be independently propagated in a communication free manner.

The forward and backward table objects contain not only the (upto) N independent forward/backward vectors at variant ℓ , but also supporting meta-data. This includes the variant the table is currently at, the scaling constants F^ℓ (forward, Equation (5)) or G^ℓ (backward, Equation (6)), the range of recipient haplotypes represented (that is, the recipient HMMs to which the column corresponds), and a hash of the parameter values used in propagating this table.

In total, a full-size forward table for example requires $8N^2 + 8N + 1576$ bytes of memory² for storage and the small overhead of R object management. Since this grows quadratically in the number of haplotypes, most functions in the package operate on

²Measured under R 4.2.2

forward and backward table objects in-place, rather than via the idiomatic copy-on-write mechanism of standard R. The most important consequence of this for users is that standard assignment of a table object to another variable name only creates a reference and so an explicit copy must be made by using the `CopyTable()` utility function provided in the package.

Core SIMD code

The two most important core algorithms which are accelerated with SIMD vector instructions are the forward and backward recursions. This code is fully implemented in C, with tailored modifications accounting for all combinations of: scalar/vector μ , scalar/matrix Π , and use of the asymmetric mutation model of RELATE [2] or not (ie 8 combinations); to ensure that minimal memory accesses are performed where possible. So, for example, scalar μ and scalar Π parameters will be faster than any other combination since these values are likely to be held in registers (or at least L1 cache) for the duration of the recursion.

Additionally, in all places where we identify SIMD instructions may be used, a macro is deployed, with a header file providing all mappings from these macros to a specific SIMD instruction for all supported instruction sets. Taking arguably the simplest non-trivial example, all `src/ExactForward*.c` and `src/ExactBackward*.c` files make use of the custom macro `KALIS_MUL_DOUBLE(X, Y)` when they need to multiply `KALIS_DOUBLEVEC_SIZE` double precision floating point values together. The file, `src/StencilVec.h` then provides definitions for these macros under each instruction set `kalis` supports (via assembly intrinsics), together with a pure C alternative. For this example, we have (with ... indicating other macro definitions):

```
// Extract from src/StencilVec.h

#if defined(KALIS_ISA_AVX512)

#define KALIS_DOUBLEVEC_SIZE 8
```

```

691 #define KALIS_MUL_DOUBLE(X, Y) _mm512_mul_pd(X, Y)
692 ...
693
694 #elif defined(KALIS_ISA_AVX2)
695
696 #define KALIS_DOUBLEVEC_SIZE 4
697
698 #define KALIS_MUL_DOUBLE(X, Y) _mm256_mul_pd(X, Y)
699 ...
700
701 #elif defined(KALIS_ISA_NEON)
702
703 #define KALIS_DOUBLEVEC_SIZE 2
704
705 #define KALIS_MUL_DOUBLE(X, Y) vmulq_f64(X, Y)
706 ...
707
708 #elif defined(KALIS_ISA_NOASM)
709
710 #define KALIS_DOUBLEVEC_SIZE 1
711
712 #define KALIS_MUL_DOUBLE(X, Y) (X) * (Y)
713 ...
714 #endif

```

The inner-most loop in these core files then includes a programmatically generated unroll to the depth specified during compilation. All this is wrapped in code which dispatches using `pthread`s to multiple threads, with automatic detection of the ability to pin to specific cores if that option is passed (important in some settings to ensure a hot L1/L2 core cache). In particular, each thread operates on a subset of columns of the forward and backward tables, ensuring spatial locality for memory accesses. Furthermore, when propagating by more than a single variant position, each column (ie each independent HMM) is propagated all the way to the target variant before proceeding to the next column, ensuing temporal locality of memory accesses.

[Unit tests](#)

Given the complexity of the development described above, we have implemented a comprehensive suite of unit tests to ensure correctness. Internal to the package is a “gold master” implementation of the LS model, which is a pure R implementation that has been written for correctness and is not optimised for speed. These pure R implementations are callable with an undocumented argument option to the standard `Forward()` and `Backward()` functions: if the argument `nthreads = "R"` rather than a numeric value, then the gold master implementation is used (at the cost of running significantly slower).

Unit tests fall broadly into two categories, one verifying the correctness of loading from the different supported input formats (via R matrix, `.hap.gz` and `h5`) into the optimised binary representation of Figure 1, the other checking forward and backward computations against a ground truth computed by the gold standard R implementation. The latter category of tests are the most extensive, since they cover tests of all combinations of: single threaded and multi-threaded computation; moving different numbers of variants in a single call; different problem sizes where the numbers of haplotypes is either exactly divisible by the CPU vector unit length (i.e. 256-bits for AVX2 etc), or has different remainders; original LS and derived allele haplotype copying model; scalar and vector mutation probabilities (μ); uniform and matrix copying probabilities (Π); and in the case of backward recursions, all combinations of starting and ending a recursion in standard or rescaled probability space (`beta.theta` argument to `Backward()`).

All these combinations give rise to over 162,000 tests (note also that the exact number of tests varies by architecture due to the differing vector unit lengths). This large number of tests ensures all the separately optimised code paths for the various combinations of run-time options are covered. We note that the tests take quite some time to run (e.g. potentially 30-60 minutes on a laptop), precisely because the gold master R code is run to provide the ground truth for these tests.

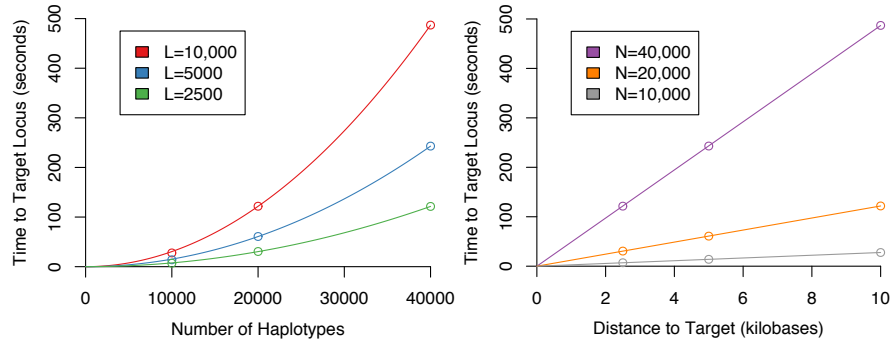


Fig. 2 **kalis** shows the expected order N^2 and order L scaling of the LS model. Computed on an Amazon Web Services c4.8xlarge instance (36 vCPUs, 60 GB of RAM).

If a user wishes to confirm correctness on their particular platform, they can be run with the following commands:

```
remotes::install_github("louisaslett/kalis",
                        INSTALL_opts = "--install-tests")
testthat::test_package("kalis")
```

Results

We provide a brief overview of some example performance figures, though due to the highly tuned nature of **kalis**, the exact performance you can expect will be heavily dependent on your exact computer architecture and resources.

First, it is important to note we do *not* claim to have altered the scaling properties of the LS model, only that we provide an implementation which is highly optimised within the scaling constraints inherent to the model. As such, Figure 2 demonstrates that **kalis** indeed inherits the $\mathcal{O}(N^2)$ and $\mathcal{O}(L)$ properties of the original LS model.

We turn now to the benefits **kalis** does provide.

Firstly, for some of the reasons highlighted in the previous Section, **kalis** exhibits accelerated performance when propagating the forward/backward recursions over more extended stretches of the genome. This is because every effort has been made to

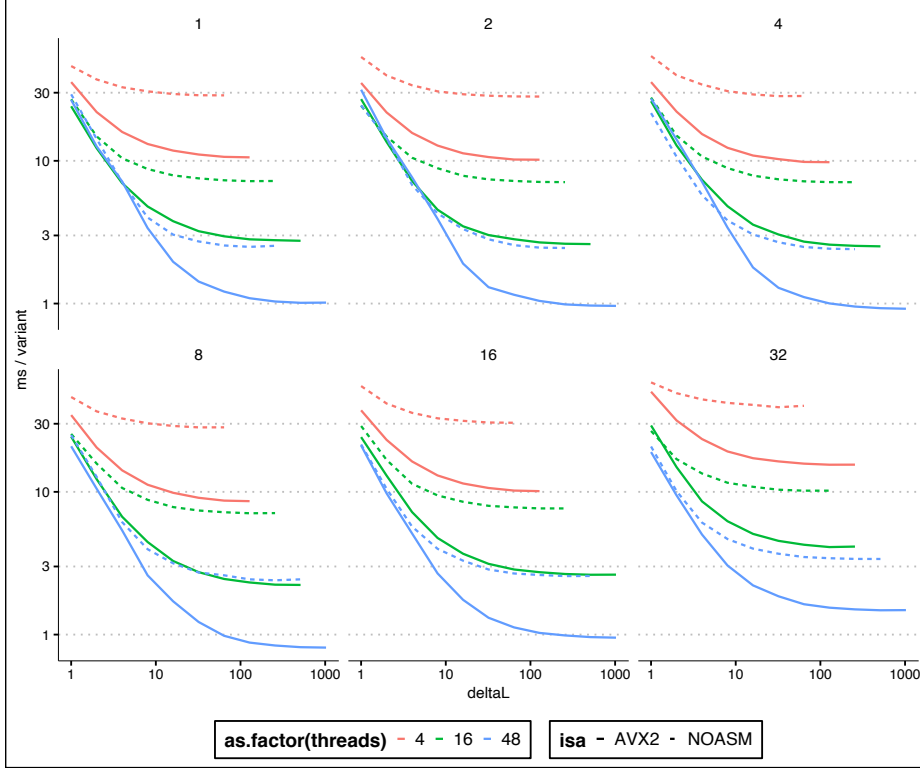


Fig. 3 Log-log plot of milliseconds per variant performance (y -axis) of the forward algorithm on 10,000 haplotypes, against the number of variants propagated (x -axis). Each panel is a different loop unrolling depth (panel title gives loop unrolling level). Line colour denotes number of CPU threads, whilst a dashed line indicates vanilla C and a solid line indicates hand-coded AVX2 instructions. In total, using AVX2, 48 threads, and loop unrolls to depth 8, it takes less than 10 seconds to propagate a 10000×10000 forward table over 10,000 variants.

be cache efficient, so that when more than a single variant step is taken, the strong cache locality design ensures that we are not memory bandwidth limited. This effect can be seen quite dramatically in Figure 3 by the rapid decrease in compute time per variant as longer stretches are propagated.

Secondly, the hard-coded loop unrolling functionality which can be controlled at compile time by the user can be seen to be beneficial in Figure 3. Clearly excessive loop unrolling is harmful, with depth 32 unrolls actually being substantially slower than no unrolling. However, unrolling to depth 8 does give a clear improvement. The best choice of unrolls will be both problem and architecture dependent, so we recommend

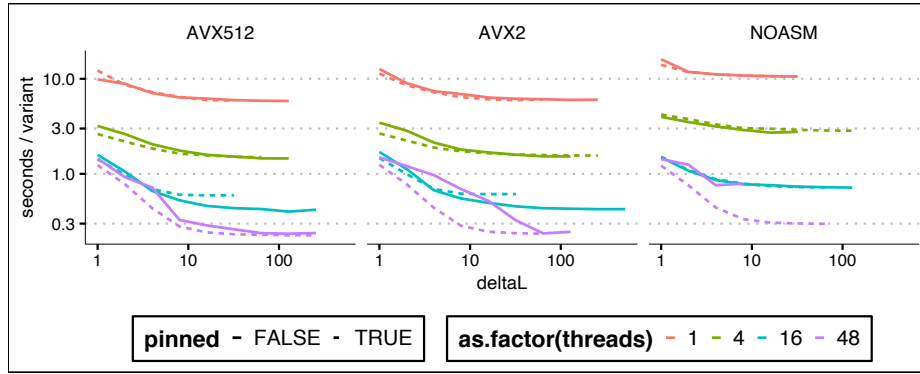


Fig. 4 Log-log plot of seconds per variant performance (y -axis) of the forward algorithm on 100,000 haplotypes, against the number of variants propagated (x -axis). Each panel is a different instruction set (AVX-512/AVX2/none). Line colour denotes number of CPU threads, whilst a dashed line indicates pinned threads and a solid line indicates no thread pinning. In total, using AVX-512, 48 threads, and pinned threads, it takes less approximately 38 minutes to propagate a 100000×100000 forward table over 10,000 variants.

testing different unroll levels on the target problem before performing long compute runs.

Figure 3 also illustrates that the hand-designed use of low-level vector SIMD instructions is not superfluous, with substantial speed-up afforded by their use (the difference between dashed and solid lines of the same colour).

Finally, Figure 4 shows that in certain very large problem settings **kalis**' ability to pin threads can make a substantial difference. In this setting, AVX2 showed the greatest benefit from eliminating context switching, ensuring that the cache is not invalidated by threads migrating between cores. The lack of substantial difference between AVX2 and AVX-512 here once thread pinning is employed calls for some investigation, though this may be a result of thermal/power throttling which is known to occur especially for AVX-512 heavy code [17].

These performance examples again highlight the importance of pilot benchmark runs with different configurations of instruction set and unroll settings before embarking on long compute runs to ensure the greatest compute efficiency is achieved for a given problem and compute architecture.

Benchmarking comparison

We performed two benchmarking experiments to compare the implementations of the forward and backward algorithms in **kalis** to those in Relate [2]. We based all of our benchmarks off on the same set of haplotypes, taken from the 1000 Genomes Project [23], as used in our real-data example which follows below. The data include 5008 haplotypes observed at 29193 variants.

kalis can perform the forward and backward recursions under either the original LS model (the default) or the derived allele haplotype copying model if `use.speidel=TRUE` is passed to the `Parameters()` function. Since Relate only computes these recursions for the derived allele copying model, it can exploit the asymmetry in the emission kernel based on the derived allele orientation of each variant. When painting a given recipient haplotype as a mosaic of donor haplotypes, this allows Relate to effectively skip all variants where a recipient haplotype does not carry the derived allele. This acceleration cannot be applied to the original LS model, which **kalis** was primarily designed for, because the symmetric emission kernel requires both the forward and backward algorithms to iterate over every variant for every recipient haplotype. Even with the derived allele copying model activated, **kalis** will still visit every variant for every recipient haplotype.

Accordingly, we found that the forward and backward recursions were approximately $4\times$ faster using Relate rather than using **kalis**. However, if Relate visits every locus, as would be necessary to compute the original LS model, we found that the forward and backward recursions were approximately $6\times$ faster using **kalis** rather than using Relate. This demonstrates the benefit of the low-level optimisations made in **kalis**. In principle **kalis** could also employ the same optimisation as Relate and visit only derived sites for every recipient haplotype. We consider this an exciting avenue of future research.

Full details of how this benchmarking was performed are provided in Additional file 1, Section D.

Real-data example: recent selection for lactase persistence

LCT is a gene on chromosome 2 that encodes lactase, the enzyme responsible for the breakdown and digestion of lactose, the sugar commonly found in milk. Ancestral humans had a regulatory ‘switch’ on chromosome 2 that stops lactase production after infancy when children would be weaned off breast milk. Mutations that disrupt this switch allow lactase production to persist into adulthood, conferring a lifelong ability to extract energy from milk [19]. Such mutations have arisen independently at least twice in human history, in Europe and in East Africa, and are among the strongest examples of recent positive natural selection in humans [20, 21]. These mutations have been shown to spread across standard human population boundaries. ~~Using~~ For example, [22] used another implementation of the LS model ~~, [22] estimated to compare haplotypes at the *LCT* locus sampled from the West African Fula population to haplotypes collected from across Europe and Asia as part of the 1000 Genomes project [23]. They found that the genetic distance between Fulani haplotypes and Eurasian haplotypes was unusually small at the *LCT* locus. With some further analysis, they interpreted this as evidence~~ that a European haplotype conferring lactase persistence became prevalent within the West African Fula population due to recent natural selection sometime over the past two thousand years.

~~Here we~~ Although it is difficult to directly replicate [22] since the Fulani samples they studied are not a part of the 1000 Genomes project, we take inspiration from their analysis. Here we present a small example using *kalis* to informally investigate whether there is evidence of recent gene-flow from Eurasia into any of the African populations in the 1000 Genomes dataset at the lactase locus. We run *kalis* on 5008 haplotypes from the 1000 Genomes Phase 3 release to revisit the haplotype structure around

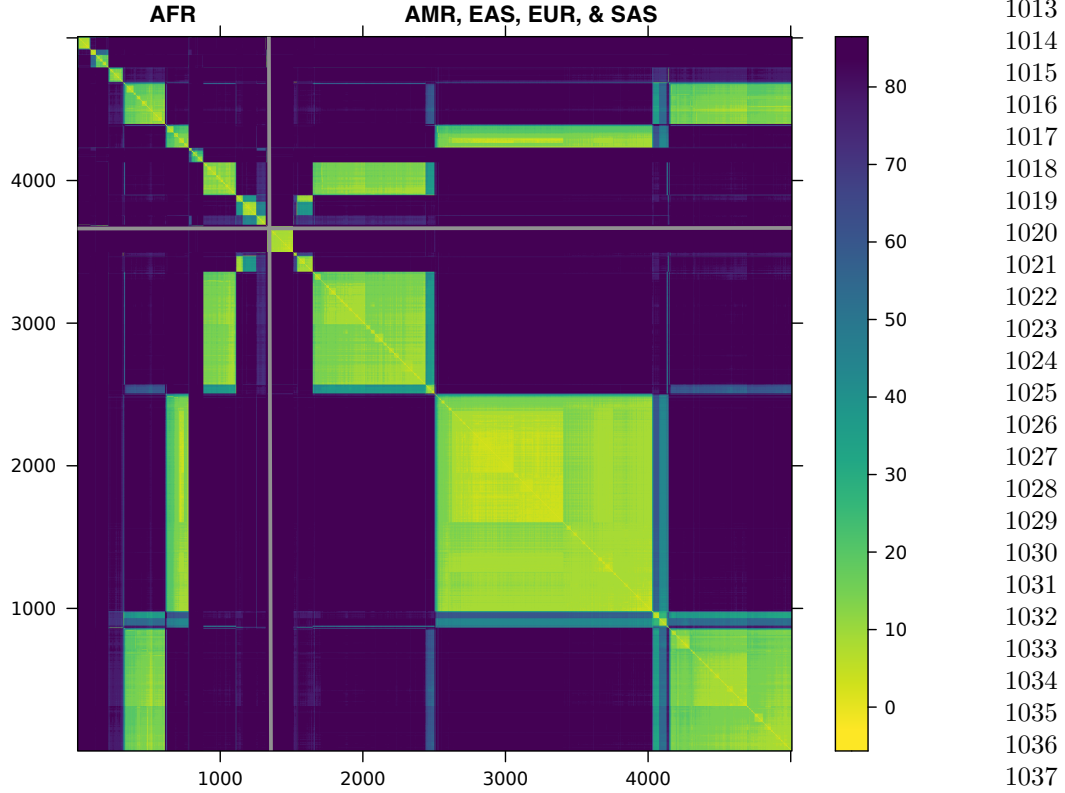


Fig. 5 Distance matrix among 5008 haplotypes calculated at **rs4988235**, upstream of *LCT*. African haplotypes are clustered in the upper left corner and separated by grey lines from non-African haplotypes from the Americas (AMR), East Asia (EAS), Europe (EUR), and SAS (South Asia). The scale on the right maps the colours to distances.

LCT; the haplotypes are sampled from 26 sub-populations all over the world [23]. Figure 5 shows a clustered version of a distance matrix, calculated as in Equation (4), at a variant in the regulatory region of *LCT* (**rs4988235**). To see if we could observe a pattern of gene-flow into or out of Africa similar to what was observed by [22], we use average pairwise linkage [24] to cluster the African haplotypes separately from the non-African haplotypes. In Figure 5, distances between African haplotypes are shown in the upper left corner; non-African haplotypes, in the lower right corner.

1059 Rather than 26 clusters reflecting the 26 sampled human populations, we see that
1060 there are three very distinct lactase haplotypes that are common both within and out-
1061 side Africa. This suggests that these three haplotypes, under strong positive selection
1062 pressure, recently spread across population boundaries and presumably confer lac-
1063 tase persistence. ~~However,~~ We cannot confirm whether any of these three haplotypes
1064 correspond to the one identified in the Fulani by [22]. These three haplotypes are not
1065 the only structure we see: in the upper left corner of the African (AFR) block we see
1066 some haplotypes that are only found inside Africa; and in the non-African block, a
1067 haplotype that is only found outside Africa. We can also see some sub-structure within
1068 the clear haplotype blocks.

1075 The code to reproduce this example is available in the
1076 examples directory of repository associated with this paper
1077 (<https://github.com/louisaslett/kalis-bmc>), as a vignette in the package
1078 (if vignettes built at install time), or directly at the **kalis** package website
1079 https://kalis.louisaslett.com/articles/lct_example.html
1080
1081

1082 Discussion

1083
1084
1085 In Additional file 2, we introduce the package from a user perspective, from package
1086 installation right through to decoding a single variant position in R using **kalis**.

1087
1088 There are many avenues for future research in developing **kalis**. On the model side,
1089 for example, allowing for different recombination rates between sub-populations as
1090 done in fastPHASE [25] would be a natural extension.

1091
1092 On the computational side, ARM scalable vector extensions [26] represent an inter-
1093 esting new approach to SIMD instruction sets, where the width of instructions need
1094 not be hard coded prior to compilation. At present it is not widely available, but as this
1095 rolls out, it would be natural to extend **kalis** to enable targeting this new instruction
1096 set.

An important utility extension is expanding the file formats that **kalis** can natively read via `CacheHaplotypes()`, to enable simpler and more streamlined software pipelines when bioinformaticians incorporate **kalis** into their workflows.

Finally, a future avenue of potential development is extension of **kalis** to support GPU or tensor cards. Note that it was an explicit design choice to initially target CPU SIMD extensions, since the vast majority of University high performance computing clusters have a huge amount of untapped compute power in this form, but often much more limited availability of specialist extension cards. Therefore, by pushing performance as extensively as possible via CPU only means, we provide the greatest potential impact for end users. This does not preclude future versions adding support for add-on compute cards.

Conclusion

kalis provides a R interface to a highly optimized C implementation of the LS model that enables local ancestry, selection, and associations studies in modern large genomic datasets.

Availability and requirements

Project name: **kalis**

Project home page: <https://kalis.louisaslett.com/>

Operating system(s): Linux, MacOS, Windows

Programming language: R, C

Other requirements: R ($\geq 3.5.0$)

License: GPL (≥ 3)

Any restrictions to use by non-academics: None beyond GPL (≥ 3).

1151 **List of abbreviations**

1152

1153 LS model = Li & Stephens model

1154

1155 HMM = hidden Markov model

1156

1157 SIMD = single instruction, multiple data

1158

1159 **Supplementary information.**

1160

1161

1162 **Declarations**

1163

1164 **Ethics approval and consent to participate.** Not applicable.

1165

1166 **Consent for publication.** Not applicable.

1167

1168

1169 **Availability of data and materials.** The package source code repository is at

1170

1171 <https://github.com/louisaslett/kalis>. All scripts for reproducing the results of this

1172

1173 paper are available in this repository <https://github.com/louisaslett/kalis-bmc>. The

1174

1175 two external dependencies are: 1000 Genomes data which are available for download

1176

1177 from <https://www.internationalgenome.org/>; and the msprime simulator, which may

1178

1179 be downloaded from <https://tskit.dev/software/msprime.html>.

1180

1181 **Competing interests.** The authors declare that they have no competing interests.

1182

1183 **Funding.** This project was supported by the NHGRI Centers for Common Disease

1184

1185 Genomics grant (UM1-HG008853), active from 2015-2022.

1186

1187 **Authors' contributions.** LA architected and wrote the C-core. LA and RC collab-

1188

1189 orated on the R interface. RC conducted the real-world lactase persistence example.

1190

1191 LA and RC wrote and approved the final manuscript.

1192

1193 **Acknowledgements.** Both authors would like to acknowledge Professor Ira Hall,

1194

1195 Professor Chris Holmes, and Dr Chris Spencer for their discussions and advice on this

1196

1197

1198

1199

1200

1201

1202

1203

1204

1205

1206

1207

1208

1209

1210

1211

1212

1213

1214

References

- [1] Li, N. & Stephens, M. Modeling linkage disequilibrium and identifying recom-
bination hotspots using single-nucleotide polymorphism data. *Genetics* **165**,
2213–2233 (2003). URL <http://www.genetics.org/content/165/4/2213>.
- [2] Speidel, L., Forest, M., Shi, S. & Myers, S. R. A method for genome-wide
genealogy estimation for thousands of samples. *Nature Genetics* **51**, 1321–1329
(2019).
- [3] Song, Y. S. Na Li and Matthew Stephens on Modeling Linkage Disequilibrium.
Genetics **203**, 1005–1006 (2016). URL [http://www.genetics.org/content/203/3/](http://www.genetics.org/content/203/3/1005)
1005.
- [4] Browning, B. L., Tian, X., Zhou, Y. & Browning, S. R.
Fast two-stage phasing of large-scale sequence data.
The American Journal of Human Genetics **108**, 1880–1890 (2021).
- [5] Rubinacci, S., Delaneau, O. & Marchini, J. Genotype imputation using the positional burrows wheeler transfo
PLoS genetics **16**, e1009049 (2020).
- [6] Kelleher, J. et al. Inferring whole-genome histories in large population datasets.
Nature genetics **51**, 1330–1338 (2019).
- [7] Lawson, D. J., Hellenthal, G., Myers, S. & Falush, D. Inference of population
structure using dense haplotype data. *PLoS genetics* **8**, e1002453 (2012).
- [8] Rosen, Y. M. & Paten, B. J. An average-case sublinear forward algorithm for the haploid Li and Stephens mo
Algorithms for Molecular Biology **14**, 1–12 (2019).
- [9] R Core Team. *R: A Language and Environment for Statistical Computing*. R
Foundation for Statistical Computing, Vienna, Austria (2023). URL <https://>

1243 www.R-project.org/.
1244
1245 [10] Sutter, H. The free lunch is over: A fundamental turn toward concurrency in
1246 software. *Dr. Dobbs's Journal* **30**, 202–210 (2005).
1247
1248
1249 [11] Peleg, A. & Weiser, U. MMX technology extension to the Intel architecture.
1250 *IEEE Micro* **16**, 42–50 (1996).
1251
1252
1253 [12] Intel Corporation. Intel Architecture Instruction Set Extensions and Future
1254 Features. Tech. Rep. 319433-046 (2022).
1255
1256
1257 [13] ARM. NEON Programmer’s Guide. Tech. Rep. DEN0018A ID071613 (2013).
1258
1259
1260 [14] Alpert, D. & Avnon, D. Architecture of the Pentium microprocessor. *IEEE Micro*
1261 **13**, 11–21 (1993).
1262
1263
1264 [15] ISO. *ISO/IEC 9899:2018 Information technology — Programming languages —*
1265 *C* Fourth edn (BSI, 2018). URL <https://www.iso.org/standard/74528.html>.
1266
1267
1268 [16] Rabiner, L. R. A tutorial on hidden Markov models and selected applications in
1269 speech recognition. *Proceedings of the IEEE* **77**, 257–286 (1989).
1270
1271
1272 [17] Schöne, R., Ilsche, T., Bielert, M., Gocht, A. & Hackenberg, D. IEEE (ed.)
1273 *Energy efficiency features of the Intel Skylake-SP processor and their impact on*
1274 *performance.* (ed.IEEE) *2019 International Conference on High Performance*
1275 *Computing & Simulation (HPCS)*, 399–406 (2019).
1276
1277
1278 [18] Consortium, . G. P. *et al.* A global reference for human genetic variation. *Nature*
1279 **526**, 68 (2015).
1280
1281
1282 [19] Ingram, C. J., Mulcare, C. A., Itan, Y., Thomas, M. G. & Swallow, D. M. Lactose
1283 digestion and the evolutionary genetics of lactase persistence. *Human genetics*
1284
1285
1286
1287
1288

	1289
	1290
	1291
[20] Ranciaro, A. <i>et al.</i> Genetic origins of lactase persistence and the spread of	1292
pastoralism in Africa. <i>The American Journal of Human Genetics</i> 94 , 496–510	1293
(2014).	1294
	1295
	1296
[21] Bersaglieri, T. <i>et al.</i> Genetic signatures of strong recent positive selection at the	1297
lactase gene. <i>The American Journal of Human Genetics</i> 74 , 1111–1120 (2004).	1298
	1299
	1300
[22] Busby, G. <i>et al.</i> Inferring adaptive gene-flow in recent African history. <i>BioRxiv</i>	1301
205252 (2017).	1302
	1303
	1304
[23] Consortium, G. P. <i>et al.</i> A global reference for human genetic variation. <i>Nature</i>	1305
526, 68 (2015).	1306
	1307
	1308
	1309
[24] Sokal, R. R. A statistical method for evaluating systematic relationships. <i>Univ.</i>	1310
<i>Kansas, Sci. Bull.</i> 38 , 1409–1438 (1958).	1311
	1312
	1313
[25] Scheet, P. & Stephens, M. A fast and flexible statistical model for large-scale pop-	1314
ulation genotype data: applications to inferring missing genotypes and haplotypic	1315
phase. <i>The American Journal of Human Genetics</i> 78 , 629–644 (2006).	1316
	1317
	1318
	1319
[26] Stephens, N. <i>et al.</i> The ARM Scalable Vector Extension. <i>IEEE Micro</i> 37 , 26–39	1320
(2017).	1321
	1322
	1323
	1324
	1325
	1326
	1327
	1328
	1329
	1330
	1331
	1332
	1333
	1334